Organic Geochemistry 132 (2019) 50–61

Contents lists available at ScienceDirect

Organic Geochemistry

journal homepage: www.elsevier.com/locate/orggeochem

A multiproxy study of past environmental changes in the Sea of Okhotsk during the last 1.5 Ma

Julie Lattaud [a,*], Li Lo [b], Christian Zeeden [c], Ya-Jun Liu [d], Sheng-Rong Song [d], Marcel T.J. van der Meer [a], Jaap S. Sinninghe Damsté [a,e], Stefan Schouten [a,e]

[a] NIOZ, Royal Netherlands Institute for Sea Research, Department of Marine Microbiology and Biogeochemistry (MMB), and Utrecht University, the Netherlands
[b] State Key Laboratory of Isotope Geochemistry, Guangzhou Institute of Geochemistry, Chinese Academy of Sciences, China
[c] LIAG – Leibniz Institute for Applied Geophysics, Geozentrum Hannover, Germany
[d] Department of Geosciences, National Taiwan University, Taiwan, ROC
[e] Utrecht University, Department of Earth Sciences, Faculty of Geosciences, Princetonlaan 8a, 3584 CD Utrecht, the Netherlands

ARTICLE INFO

Article history:
Received 17 December 2018
Received in revised form 23 March 2019
Accepted 10 April 2019
Available online 12 April 2019

Keywords:
Sea of Okhotsk
Mid-Pleistocene Transition
LDI
TEX_{86}
$U^{k'}_{37}$
Biogenic opal
Long-chain diols

ABSTRACT

Long-chain diols have been detected in a wide range of environments and have been used to reconstruct past environmental changes, however only a few long-term records exist to date. Here we reconstructed past environmental changes in the central Sea of Okhotsk over the last 1.5 million years, covering the Mid-Pleistocene Transition (MPT). Sea surface temperatures (SST) reconstructed using the Long-Chain Diol Index (LDI) reflects glacial/interglacial changes. However, when compared with other organic paleothermometers ($U^{k'}_{37}$ and TEX^{L}_{86}) the LDI-SST is lower during interglacials and similar or higher during glacials, possibly suggesting a shift of diol production season during interglacials. The LDI-SST does not change in periodicity around the MPT as observed for the TEX^{L}_{86}, likely due to this seasonal shift. Diatom productivity, as recorded by 1,14-diols and biogenic opal content, increased during the main deglaciations with a succession from *Proboscia* diatoms to diatoms with a more heavily silicified shell, confirming that primary productivity in the central Sea of Okhotsk is driven by sea-ice progress and retreat. In contrast to the LDI-SST, the 1,14-diols record shows a change in periodicity around the MPT from 41- to 100-kyr cycle, suggesting an influence of orbital parameters on diatom productivity. In the central Sea of Okhotsk, the relative amount of C_{32} 1,15-diol ($F_{C32\ 1,15}$), a proxy for riverine input, correlates with sea-level change with more riverine-derived material reaching the core site when the Amur River mouth is closer at lower sea-levels. In agreement, $F_{C32\ 1,15}$ shows a change in periodicity during the MPT, with the appearance of a 100-kyr cycle. Our results show that the long chain diols can provide important paleoceanographic information in subpolar environments over long time scales, but that temperature reconstructions can be severely impacted by changes in seasonality.

1. Introduction

The last 2 million years (Ma) in the Earth history cover an important climatic transition called the Mid-Pleistocene Transition (MPT) where the start of pronounced glacial/interglacial successions was initiated. This MPT occurred around ~950 ka, with a change in the dominant periodicity from 41- to 100-kyr as seen in benthic foraminifera $\delta^{18}O$ records (Lisiecki and Raymo, 2005). At the same time, an overall positive isotope shift in these records is observed, due to more severe and longer glaciations (e.g. Hays et al., 1976; Shackleton and Opdyke, 1976; Pisias and Moore, 1981; Clark and Pollard; 1998; Berger et al., 1999; Medina-Elizalde and Lea, 2005; Clark et al., 2006; Elderfield et al., 2012; McClymont et al., 2013 and reference therein). The MPT was accompanied by a decrease in sea surface temperature (SST) in the northern Atlantic and an increase in aridity over the African and Asian peninsulas (Clark et al., 2006). A cold event at the start of the intensification of the glaciations (~900 ka) has been observed in several marine records (Schefuß et al., 2004; Medina-Elizalde and Lea, 2005; Elderfield et al., 2012; McClymont et al., 2013). Furthermore, the high-latitude areas underwent major changes during the MPT as the Laurentide ice sheet became volumetrically larger (Clark and Pollard, 1998). Only a few records document changes in SST during the MPT in the northern Pacific (Raymo et al., 1990; McClymont et al., 2008; Martinez-Garcia et al., 2010).

The Sea of Okhotsk is a semi-enclosed marginal sea from the northwestern Pacific and is linked to the Sea of Japan and the

* Corresponding author.
E-mail address: Julie.lattaud@nioz.nl (J. Lattaud).

https://doi.org/10.1016/j.orggeochem.2019.04.003
0146-6380/

Pacific Ocean, with the Amur River discharging terrigenous input into the eastern part. The oldest paleoceanographic record of the Sea of Okhotsk goes back to 1.1 Ma (Nürnberg and Tiedemann, 2004) and showed that the sediments from the Sea of Okhotsk reflect glacial/interglacial variability that are characteristic for the northern hemisphere (Lisiecki and Raymo, 2005). However, most sediment records of the Sea of Okhotsk only cover the late Quaternary (Gorbarenko, 1996; Sorokin and Sorokin, 1999; Ternois et al., 2001; Gorbarenko et al., 2004, 2007, 2010, 2012, 2014; Harada et al., 2004, 2006, 2008, 2012, 2014; Seki et al., 2004a, 2004b, 2009, 2012, 2014a, 2014b; Sakamoto et al., 2005, 2006; Liu et al., 2006; Wang and Wang, 2008; Ishawatari et al., 2009; Malakhov et al., 2009; Katsuki et al., 2010; Nürnberg et al., 2011; Iwasaki et al., 2012; Khim et al., 2012; Nakanowatari et al., 2014; Bosin et al., 2015; Lembke-Jene et al., 2018).

Recently, Lattaud et al. (2018) showed that organic proxies could be applied to reconstruct sea water temperatures in the Sea of Okhotsk until Marine Isotope Stage (MIS) 6 (~180 ka). In particular, they used long-chain diols (LCDs) to reconstruct past autumn SST via the Long Chain Diol Index or LDI (Rampen et al., 2012). The LDI is based on the ratio of C_{30} 1,15-diol versus 1,13-diols and has been shown to relate strongly to sea surface temperature (Rampen et al., 2012). These LCDs are thought to be produced by eustigmatophytes (Volkman et al., 1992). The presence of LCDs raises the possibility to reconstruct other parameters such as riverine input using the proportion of C_{32} 1,15-diol ($F_{C32\ 1,15}$, Lattaud et al., 2017a,b). The C_{32} 1,15-diol is the main LCD in rivers but in much lower abundances in open oceans and thus its relative abundance is a useful proxy to trace riverine input (Lattaud et al., 2017b). In addition to 1,13- and 1,15-diols, 1,14-diols are often present in marine sediments and are mainly derived from *Proboscia* diatoms. Thus, the abundance of 1,14-diols allows the reconstruction of *Proboscia* diatom productivity (Rampen et al., 2014) or possibly even upwelling intensity or high nutrient conditions (with the Diol Index or DI, Willmott et al., 2010) as these species are often found in upwelling areas and high nutrient conditions, respectively (Sundström, 1986; Sinninghe Damsté et al., 2003; Rampen et al., 2007). However, the above discussed LCD proxies have rarely been applied on long time scales, e.g. the longest LDI-SST record is dating back to 3.3 Ma in sapropels from the Mediterranean Sea (Plancq et al., 2015) but most records do not go further back than 180 ka (Lopes dos Santos et al., 2012; Smith et al., 2013; Jonas et al., 2017; Kotthoff et al., 2017; Lattaud et al., 2017b, 2018; Warnock et al., 2017, De Bar et al., 2018).

In this study we extended the LDI-SST record in the Sea of Okhotsk to 1.5 Ma to fully capture the MPT. Furthermore, we applied other LCD proxies, i.e. $F_{C32\ 1,15}$ (to trace river input; Lattaud et al., 2017a), the DI and the 1,14-diols (as *Proboscia* diatom indicator), to reconstruct environmental changes during the MPT in the central Sea of Okhotsk. These LCD proxy records were compared with other sea water temperature proxies (TEX^L_{86} reflecting summer subsurface temperatures and $U^{k'}_{37}$ reflecting autumn SST; Lattaud et al., 2018) as well as with productivity proxies such as biogenic opal content, and riverine input proxies such as the hydrogen isotopic composition of long chain alkenones, reflecting the hydrogen isotopic composition of the water and salinity, and the Branched versus Isoprenoid Tetraether (BIT) index.

2. Material and methods

2.1. Study site

The Sea of Okhotsk is part of the Western Pacific Ocean and it is the southernmost sea of the northern hemisphere with seasonal sea-ice cover (Harada et al., 2014). Nowadays, polynyas open up on the northeastern shelf area and can spread to cover up to 85% of the Sea of Okhotsk (Hays and Morlet, 2003). It is a highly productive sea with a major planktonic spring bloom and a smaller autumn bloom of diatoms (Hays and Morlet, 2003). In autumn there is also a major haptophyte bloom with *Coccolithus oceanicus* and *Emiliana huxleyi* (Broerse et al., 2000). In the Sea of Okhotsk, autumn SST, salinity and sea-ice extend, influence the intensity of downwelling that creates the Okhotsk Sea Intermediate Water (OSIW), which in turn is a key component of the North Pacific Intermediate Water (NPIW) (Tsunogai et al., 1992).

Giant piston core MD01-2414 (53°11.77′N, 149°34.80′E and water depth of 1123 m, Fig. 1) was collected during the IMAGES VII cruise from the central region of the Sea of Okhotsk (Deryugin basin) as described by Chou et al. (2011). This core has a length of 52.76 m and we studied the top 51 m. The age model is described in Lo et al. (2018) and was obtained by correlating the XRF core scanner data with the global $\delta^{18}O$ LR04 stack (Lisiecki and Raymo, 2005). Furthermore, 5 radiocarbon ^{14}C ages of planktonic foraminifera (*Neogloboquadrina pachyderma*, *sinistral*) were determined by accelerator mass spectrometry (AMS). Together this shows that the core covers ages between 3.7 and 1520 ka with sedimentation rates varying between 1 and 4 cm kyr^{-1}. The sediment core was sampled every 10 cm which corresponds to a time resolution of 3- to 10-kyr, and the sediment was stored frozen until freeze-dried. Besides the piston core samples, thirteen surface sediments were collected from the Sea of Okhotsk as described by Lo et al. (2018).

2.2. Extraction and separation of lipids

The sediments were extracted following the procedures described by Lo et al. (2018). Briefly, sediment samples (1–10 g) were homogenized, freeze-dried and extracted using dichloromethane (DCM):methanol (MeOH) (4:1, v/v) using an Accelerated Solvent Extractor (ASE). The extracts were separated into three fractions on a Pasteur pipette packed with activated Al_2O_3: an apolar fraction (hexane:DCM, 9:1 v/v), a ketone fraction (hexane:DCM, 1:1 v/v) containing alkenones, and a polar fraction (DCM:MeOH, 1:1 v/v) containing the Glycerol Dialkyl Glycerol Tetraethers (GDGTs) and long-chain diols were obtained.

2.3. Analysis of biomarkers

The alkenone and LCDs were analysed as described in Lattaud et al. (2018) and the GDGTs as described in Lo et al. (2018). A previous surface sediment study of the Sea of Okhotsk showed that TEX^L_{86} values correlated strongly with summer sea water temperature (SWT) at 20 m depth (Lattaud et al., 2018; Lo et al., 2018) and that the global calibration of Kim et al. (2010; Eq. (1)) could be used to reconstruct these temperatures. The same surface sediment study showed that $U^{k'}_{37}$ values correspond to autumn sea surface temperature (Lattaud et al., 2018) and that the $U^{k'}_{37}$ the calibration from Prahl and Wakeham (1987; Eq. (2)), which is the one most commonly applied in the Sea of Okhotsk, can be used. Finally, for the LDI, the regional core-top calibration to autumn-SST from Lattaud et al. (2018) (Eq. (3)) was applied.

$$TEX^L_{86} - SWT = 67.5 \times TEX^L_{86} + 46.9 \quad (1)$$

$$U^{k'}_{37} - SST = \frac{\left(U^{k'}_{37} - 0.044\right)}{0.033} \quad (2)$$

$$LDI - SST = \frac{LDI + 0.29}{0.103} \quad (3)$$

The BIT index (Hopmans et al., 2004), an indicator of terrigenous input transported by rivers into the marine environment, is based on the ratio of branched GDGTs (brGDGTs, produced in riv-

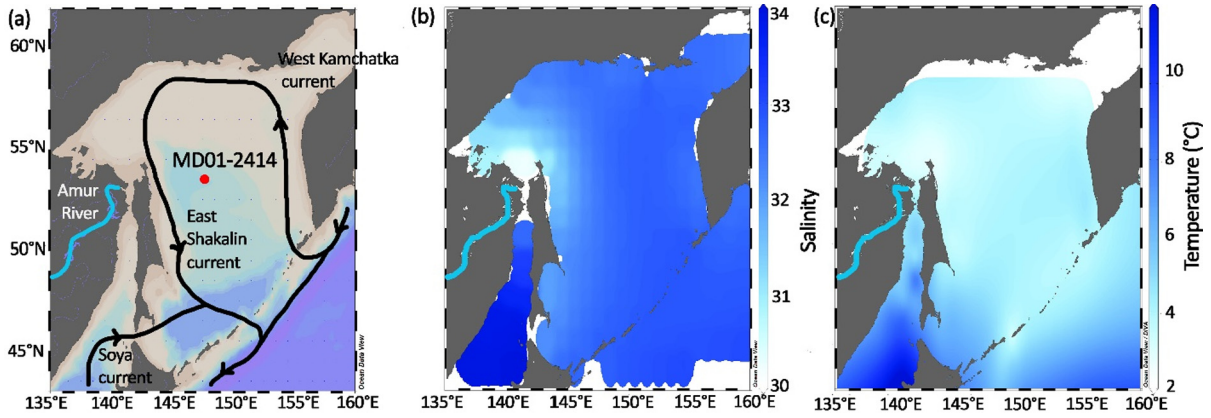

Fig. 1. (a) Location of core MD01-2414 (Lo et al., 2018) and environmental parameters of the Sea of Okhotsk with (b) annual mean surface salinity (from NOAA, Antonov et al., 2010) and (c) annual mean sea surface temperature (from NOAA, Locarnini et al., 2010).

ers and in soils, Weijers et al., 2009; De Jonge et al., 2014) over crenarchaeol (mainly produced in marine environments). The BIT index was calculated for the whole record to assess terrigenous input. Furthermore, two diol proxies were used, the $F_{C32\ 1,15}$ based on the fractional abundance of the C_{32} 1,15 diol over the C_{30} 1,15-, C_{30} 1,13- and C_{28} 1,13-diols (Lattaud et al., 2017a) and the DI based on the ratio of 1,14-diols over the C_{30} 1,13- and C_{28} 1,13-diols (Willmott et al., 2010) in order to reconstruct riverine input and nutrient conditions, respectively.

2.4. Analysis of δD of alkenones

47 sediment samples contained alkenones in high enough abundance for hydrogen isotope measurements. To analyse the δD of alkenones, the ketone fractions were dissolved in ethyl acetate and analyzed for hydrogen isotopes as described by Kasper et al. (2015). Briefly, the ketone fractions were injected on a Thermo Finnigan Delta ^{Plus} XL Gas Chromatography Thermal Conversion isotope ratio Mass Spectrometer (GC/TC/irMS). The H_3^+ correction factor was determined daily and ranged between 3.56 and 3.9. Isotopic values for alkenones were standardized against pulses of H_2 reference gas, which was injected three times at the beginning and two time at the end of each run. A set of standard *n*-alkanes with known isotopic composition (Mixture B, prepared by Arndt Schimmelmann, University of Indiana) was analyzed daily prior to each sample batch in order to monitor the system performance. Samples were only analyzed when the alkanes in Mix B had an average deviation from their off-line determined values of less than 5‰. The 47 hydrogen isotope values of alkenones (δD_{C37}) were measured as the combined peak of the $C_{37:2}$ and $C_{37:3}$, which correlates best with salinity (van der Meer et al., 2013), and 0.2 μL of a standard mixture of known δD value, composed of squalane and C_{30} n-alkane, was coinjected to each sample. The samples were analyzed in duplicate and standard deviation of duplicate analyses varied from 0 to 5‰.

2.5. Biogenic opal analysis

The opal content was measured as described by Liu et al. (2006) to extend the previous record (0–500 ka) reported by Liu et al. (2006) to 1550 ka. Briefly, freeze-dried sediments were homogenized in a mortar, and they were then smeared gently on glass slides for the mineralogical analysis. The mineralogy of the sediments was analyzed using a Science Mxp III X-ray diffractometer (MAC) with CuKα radiation. Scans of bulk powders were run at 35 kV and 15 mA over a scanning range of 3–70°.

2.6. Spectral analysis

The proxy records were linearly resampled to get an even spaced record and a 95% confidence level was chosen. A Morlet Wavelet analysis of the different records was realized with the PAST software (Hammer et al., 2001) to study the changes of periodicity in the proxy records over time.

3. Results

3.1. Temperature proxies

Using the local LDI-autumn SST calibration of Lattaud et al. (2018) we reconstructed SST using the LDI which varied from 3 to 12 °C (Fig. 2b). The LDI temperatures were 5 °C at 1520 ka, then increased to 12 °C at 1300 ka, and remained this high until 1130 ka, and then decreased until 3 °C at 1100 ka. LDI-SST were then warming reaching 9 °C at 1070 ka then decreased to 3 °C at 970 ka. This was followed by two short-termed warming events (reaching 7 °C at 960 and 930 ka). The LDI-SST was then varying by just 2 °C over the next 600 ka, with some warming events at 860 ka (MIS 21), 800 ka (MIS 19) and 400 ka (MIS 11) (reaching 7 °C, 8 °C and 8 °C, respectively). This was followed by two cycles of cooling/warming when temperatures reached a maximum of 7 and 8 °C (at 340, i.e. MIS 9 and 245 ka, i.e. MIS 7, respectively) and minimums of 3 and 4 °C. The last 180 ka (from Lattaud et al., 2018), showed that MIS 6 was characterized by low temperatures (average 5 ± 1 °C), that was followed by warmer temperatures, reaching 9 °C at 130 ka (MIS 5e). After a cooling, the most recent part of the core varied around 4-5 °C.

The $U^{k'}_{37}$-SST ranged from 1 to 23 °C (Fig. 2c) over the whole record. At 1520 ka, temperatures were around 6 °C and increased to 20 °C at 1320 ka and 23 °C at 1280 ka, then decreased to 7 °C around 1190 ka. The record was then characterized by several cooling/warming events, with the main warmings around 1160, 1070, 950, 880, 620 (MIS 15), 410 (MIS 11), 260 (MIS 8), 140 (MIS 6) and 9 ka, respectively. Late MIS 6 is characterized by relatively high temperatures (maximum of 20 °C) that remain high throughout MIS 5e (15 °C). $U^{k'}_{37}$-SST then decreased to 2.5 °C at 90 ka (MIS 5b), followed by a warming (8 °C at 80 ka). A cooling then occurred during MIS 4-2 (average of 4 °C during 70–14 ka) and the Holocene is characterized by a warming to 7 °C at 4 ka.

For TEX^{L}_{86} we used the global calibration of Kim et al. (2010) which in the Sea of Okhotsk has been shown to reflect summer subsurface sea water temperature (SWT). TEX^{L}_{86}-SWT varied from −3 to 18 °C (Fig. 2d). At 1520 ka, the TEX^{L}_{86}-SWT were 6 °C, increasing to

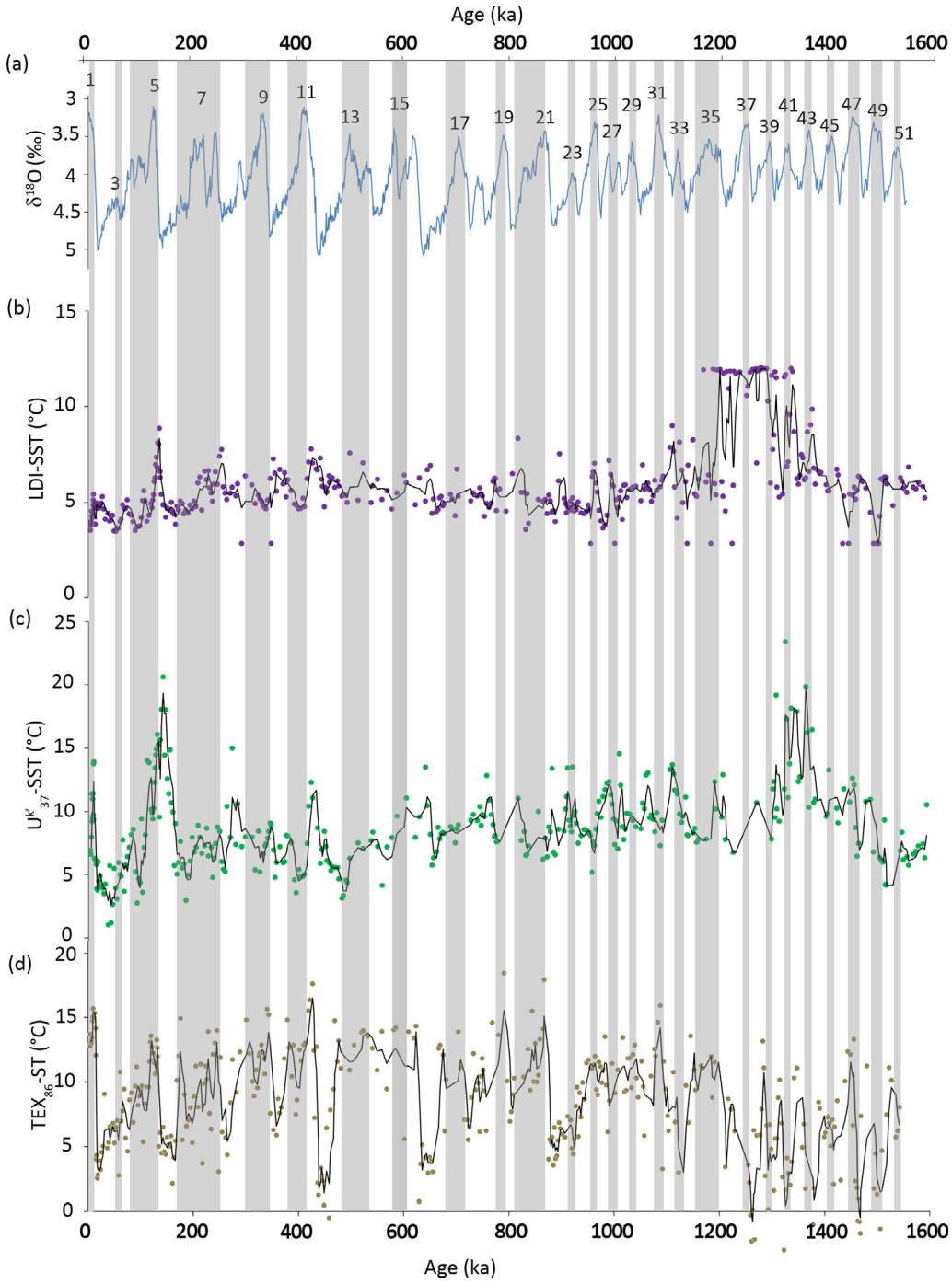

Fig. 2. Paleotemperature records for the Sea of Okhotsk (a) global stack of $\delta^{18}O$ of benthic foraminifera (Lisiecki and Raymo, 2005) with numbers indicating the different Marine Isotope Stages, and 3 point averaged temperature records of (b) LDI, (c) $U^{K'}_{37}$, (d) TEX^{L}_{86} temperatures and (e) all three temperature proxies (3-points averaged) from MD01-2414 core from the central Sea of Okhotsk. Grey bars indicate the interglacials, numbers indicates Marine Interglacials (MIS) from Lisiecki and Raymo, 2005.

16 °C until 1080 ka. This was followed by a decrease until 880 ka (TEX^{L}_{86}-SWT = 4 °C), then a rapid warming happened with TEX^{L}_{86}-SWT reaching 18 °C at 860 ka. This pattern of slow cooling and fast warming was repeated again between 860 and 620 ka and temperature ranged between 3 °C at 640 ka to 14 °C at 620 ka. This was followed by a period of relatively stable TEX^{L}_{86} temperatures (8.5 ± 2 °C, n = 15) until 470 ka, followed by a steep cooling with TEX^{L}_{86}-SWT reaching −1 °C at 460 ka (MIS 12). After MIS 12, a relatively fast warming was observed with TEX^{L}_{86} temperatures increasing to the warmest temperature of the record of 18 °C at 430 ka (MIS 11). This was followed by a slow cooling until 150 ka (4 °C) (MIS 6). At 130 ka (MIS 5e) the TEX^{L}_{86} temperature reached 13 °C which decreased until 3 °C at 20 ka (MIS 2), respectively (Lo et al., 2018).

3.2. Riverine input proxies

The $F_{C32\ 1,15}$, a proxy for riverine input (Lattaud et al., 2017a), ranged from 0.1 to 0.7 in the sediment core (Fig. 3). Between 1520 and 1250 ka $F_{C32\ 1,15}$ was stable around 0.4 ± 0.1 (n = 73), except for a sharp drop (down to 0.2) at 1450 ka, then decreased to 0.1 between 1250 and 1150 ka, followed by an increase until 0.5 at 1140 ka. $F_{C32\ 1,15}$ decreased rapidly to 0.2 at 1070 ka before

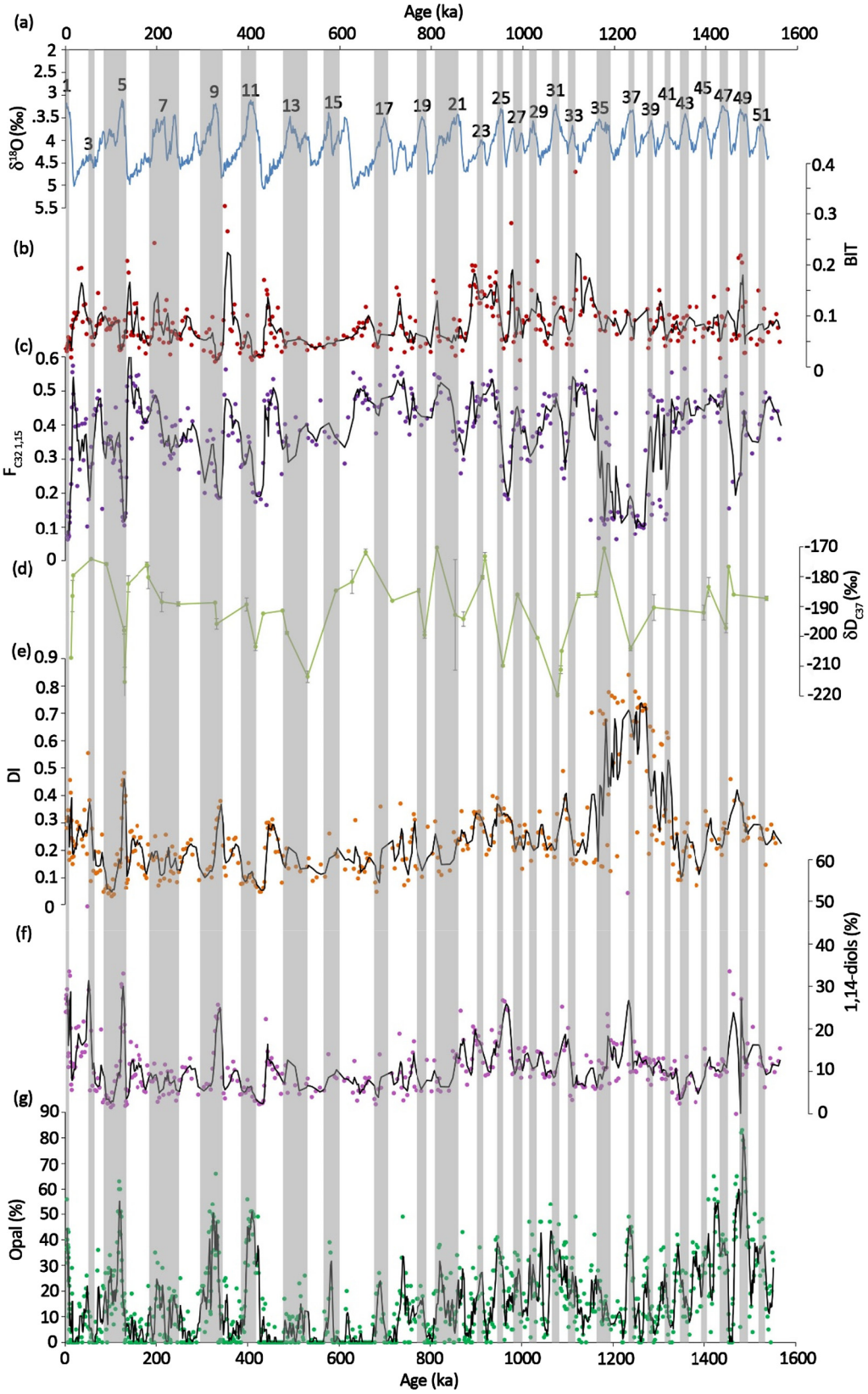

Fig. 3. (a) The $\delta^{18}O$ benthic foraminifera global stack (Lisiecki and Raymo, 2005) with numbers indicating the different Marine Isotope Stages, and proxy records of the Sea of Okhotsk (b) BIT index, (c) $F_{C32\ 1,15}$, (d) δD_{C37} (the grey bars represent the standard deviation of the replicate), (e) Diol Index (DI), (f) 1,14-diols in fractional abundance of all diols and (g) opal percentage (Liu et al., 2006 and this study). The black lines represents a running mean of 3 points. Grey bars indicate the interglacials, numbers indicates Marine Interglacials (MIS) from Lisiecki and Raymo, 2005.

going back to higher values (0.4) between 1060 and 960 ka, followed by a rapid decrease at 950 ka (0.2). $F_{C32\ 1,15}$ was then varying between 0.3 and 0.7 with minima around 850, 760, 600, 420, 330, 120 ka (MIS 21, 19, 15, 11, 9 and 5, respectively) and the end of the Holocene. The BIT index (Fig. 3), a proxy for riverine terrigenous input (Hopmans et al., 2004; Zell et al., 2013, 2015), had values which were generally low with an average of 0.08 ± 0.05 (n = 384) and with 0.38 as maximum at 340 ka, and the record is characterized by several brief periods with relatively high values around 1450, 1120, 920, 430 (MIS 12), 340 (MIS 10), 190 (MIS 6), 130 (MIS 5) and 36 ka (MIS 3). For comparison $F_{C32\ 1,15}$ and the BIT index was also measured in surface sediments distributed around the Sea of Okhotsk (Table 1). In the surface sediments, $F_{C32\ 1,15}$ varied between 0.02 and 0.3 and the BIT index between 0.02 and 0.12 with no particular pattern (Table 1).

3.3. Diol index

The 1,14-diols, biomarkers for *Proboscia* diatoms (Sinninghe Damsté et al., 2003; Rampen et al., 2014), were present throughout the record, and comprise on average 12 ± 0.1% of all diols (n = 409), with values ranging between 2 and 50% (Fig. 3). At 1520 ka, the 1,14-diols were 10% of all LCDs, then increased briefly to 30% at 1450 ka before going back to 10%. At 1230 ka, a sharp and brief increase in the amount of 1,14-diols took place (reaching 50% of all LCDs) before going back to previous values of 10% until 1100 ka when it increased to 20%. The 1,14-diols showed maxima at around 950, 850, 750, 720, 430, 330, 130 and 50 ka (MIS 25, 21, 17, 12, 9, 5 and 3, respectively, Fig. 3). The Diol Index (DI), an index used to reconstruct *Proboscia* productivity based on the amount of 1,14-diols versus 1,13-diols (Willmott et al., 2010), varied between 0.04 and 0.84 and showed a similar trend as that of percentage of 1,14 diols, except between 1300 and 1100 ka when the DI was continuously high (around 0.7). Between 1100 and 131 ka DI was on average 0.21 ± 0.09 (n = 228), after 131 ka the values were increasing to 0.48 at 125 ka then decreased and reached 0.04 at 100 ka. The DI was then rising until the Holocene, reaching 0.32 at 4 ka. Maxima are observed at 440, 330, 130 and 50 (MIS 12, 9, 5 and 3, respectively, Fig. 3). Finally, in the surface sediments, the DI varied between 0.26 and 0.53 and the 1,14-diols between 21 and 44% with no particular spatial patterns (Table 1).

3.4. Hydrogen isotopic composition of C_{37} alkenones

The hydrogen isotopic composition of C_{37} alkenones (δD_{C37}), a proxy for salinity (Schouten et al., 2006), was obtained in a lower resolution than the other records due to the often relatively low abundance of alkenones, too low for hydrogen isotope analysis. The δD_{C37} varied from −215‰ to −172‰, with more depleted values during interglacials. At 1520 ka the value was −187‰ then it decreased to −197‰ at 1439 ka. It was followed by an increase up to −190‰ at 1280 ka, a decrease down to −205‰ at 1076 ka an increase up to −170‰ at 807 ka (MIS 20) followed by a steep decrease until −214‰ at 523 ka (MIS 13). A slow increase took place from 523 to 83 ka (MIS 13 to MIS 5), until the δD_{C37} reached −170‰. This increase was interrupted by a short event where values briefly decreased to −215 ± 5‰ at 122 ka (MIS 5e). At the start of the Holocene at 12 ka the δD_{C37} shows a slow decrease, until −207‰ at 6 ka.

3.5. Spectral analysis

We performed wavelet analysis (using a Morlet wavelet) on nearly all of our records (Fig. 4) in the time domain, and for comparison also on the LR04 benthic foraminifera stack (Lisiecki and Raymo, 2005; reflecting global ice volume changes and deep-sea temperature), and a $U^{k'}_{37}$-SST record from the northern Pacific (Martinez-Garcia et al., 2010). The TEX_{86}-SWT record shows changes from a dominant 41-kyr cyclicity in the oldest part of the core to a dominant 100-kyr cycle in the most recent part of the core, similar to the LR04 benthic $\delta^{18}O$ stack (Fig. 4). It also has a significant 60-kyr cyclicity that appears in the last 900 ka (Fig. S1c). The LDI-SST does not show any significant cycle over the record, and the $U^{k'}_{37}$-SST record has two periods with a significant cycle of 100-kyr (around 300 to 0 ka and 1300 to 1100 ka) and 150- and 70-kyr cycles in the last 900 ka (Fig. S1). The riverine input proxy $F_{C32\ 1,15}$ shows a significant 100-kyr cycle in the younger part of the core (after 1100 ka), similar to the LR04 benthic $\delta^{18}O$ stack and multiple high frequencies peaks after 900 ka (i.e. 23-, 21- and 19-kyr, Fig. S1). For the BIT index, a 100-kyr cycle is apparent before 1100 ka as well as 75-, 50- and 41-ky cycles in the last 900 ka. For the opal content and 1,14-diols, a 100-kyr cycle is observed after 600 ka and for the opal content record, a 41-kyr cycle is present in the periods older than 1100 ka

4. Discussion

4.1. Sea water temperature evolution of the Sea of Okhotsk over the last 1.5 Ma

4.1.1. Comparison of sea water temperature proxies

Lattaud et al. (2018) showed, using surface sediments from the Sea of Okhotsk, that the three temperature proxies, LDI, $U^{k'}_{37}$, and TEX^{L}_{86}, all reflect a different season and/or depth of production, i.e. summer subsurface temperature for TEX^{L}_{86} and autumn SST for LDI and $U^{k'}_{37}$. With this in mind we compared the three temperature records. The LDI-SST is significantly correlated with $U^{k'}_{37}$-SST ($r = 0.39$, $p < 0.005$) over the whole record but not with TEX^{L}_{86}-SWT ($r = -0.1$, $p = 0.09$). Moreover, there is no correlation between TEX^{L}_{86}-SWT and $U^{k'}_{37}$-SST ($r = 0.012$, $p = 0.71$). This indicates that $U^{k'}_{37}$-SST

Table 1
LCD proxies Diol Index and $F_{C32\ 1,15}$ as well as the BIT index for surface sediments in the Sea of Okhotsk.

Name	Latitude (°N)	Longitude (°E)	DI	$F_{C32\ 1,15}$	1,14-diols (%)	BIT
55-14-2	56.07	153.68	0.53	0.15	43.5	0.02
55-17-2	56.31	146.84	0.39	0.07	35.7	0.02
55-18-2	56.34	145.31	0.38	0.03	36.9	0.02
55-23-2	53.01	146.51	0.30	0.10	25.1	0.12
55-25-2	52.56	146.51	0.31	0.10	26.5	0.06
55-27-2	52	144.56	0.28	0.20	20.8	0.03
55-30-2	52	144.94	0.36	0.10	31.1	0.03
55-34-2	48.81	147.87	0.32	0.11	22.4	0.02
55-36-2	48.58	146.36	0.29	0.15	20.1	0.03
55-44-2	47.52	145.16	0.26	0.33	13.6	0.11
55-46-2	45.51	144.54	0.34	0.18	18.3	0.04
55-47-2	45.52	144.47	0.29	0.21	14.8	0.05

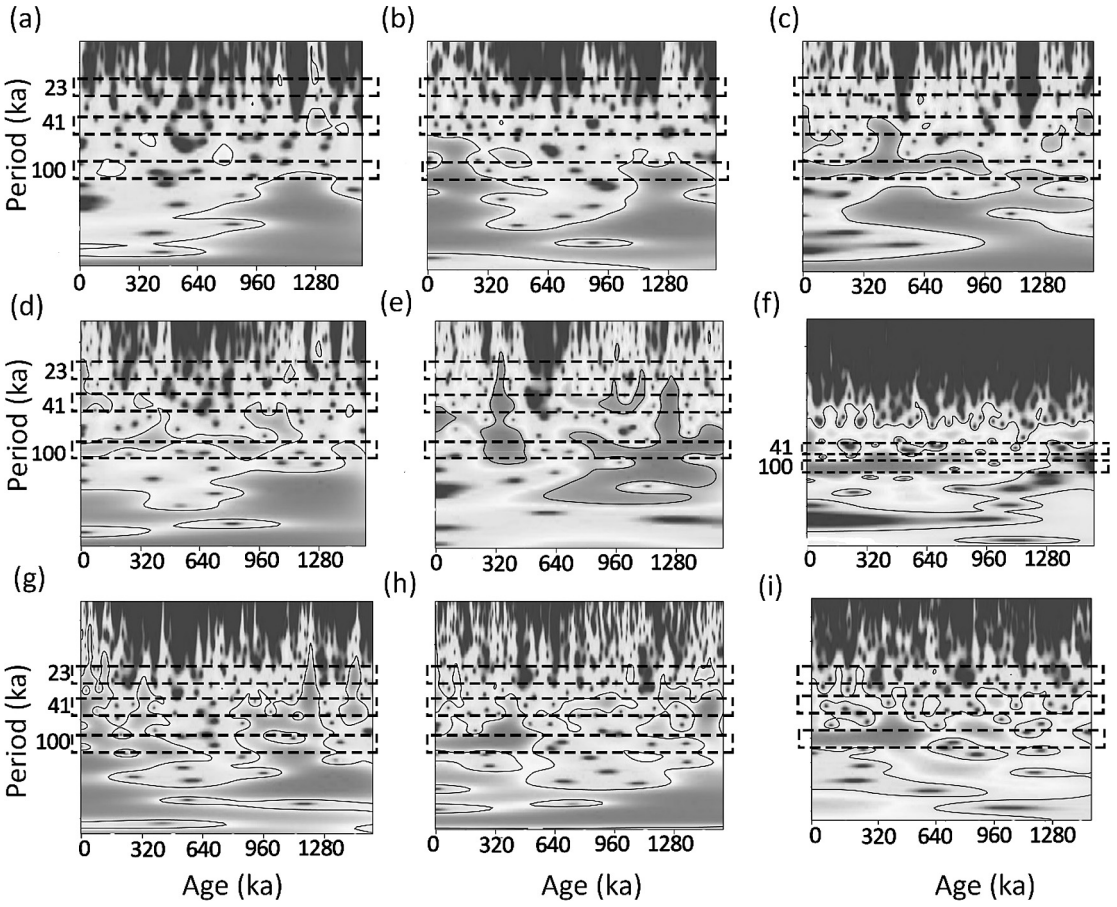

Fig. 4. Spectral analysis (Wavelet) for (a) LDI-SST, (b) $U^{k'}_{37}$-SST, (c) TEX_{86}-SST, (d) $F_{C32\ 1,15}$, (e) BIT, (f) $\delta^{18}O$ benthic foraminifera global stack (Lisiecki and Raymo, 2005), (g) 1,14-diols, (h) opal content and (i) $U^{k'}_{37}$-SST from the northern Pacific ODP Hole 806B (Martínez-Garcia et al., 2010). The black boxes show the three main orbital cycles, i.e. 23-, 41- and 100-kyr.

and LDI-SST are following a similar pattern likely reflecting autumn SST, as shown previously in Lattaud et al. (2018). The TEX^{L}_{86}-SWT is often higher than the other two proxy temperatures, except before 1200 ka when TEX^{L}_{86}-SWT are lower than the other two.

Despite the significant correlation there is still quite some discrepancy between SSTs derived from the $U^{k'}_{37}$ and LDI in both patterns as well as absolute values with the LDI often being lower (Fig. 2). Potential biases that could explain the different patterns and lower LDI-SSTs values compared to $U^{k'}_{37}$ are 1,13-diols production by *Proboscia* diatoms (Rodrigo-Gamiz et al., 2015), the influence of riverine LCDs (de Bar et al., 2016; Lattaud et al., 2017a), and a shift in the season of production toward colder months (e.g. early spring) during ice-free interglacials. Examination of the SST records shows that colder LDI temperatures are not linked with elevated amounts of 1,14-diols or higher values of $F_{C32\ 1,15}$ (Fig. 3c and 3f) indicating no influence of *Proboscia* diatoms or riverine input, respectively. This suggests that observed differences might be linked to a shift of production of long-chain diols towards a colder season like early spring or late autumn due to longer summer and ice-free conditions during interglacials. This hypothesis was also used to explain the colder LDI-SST compared to $U^{k'}_{37}$-SST observed in the last 180 ka of the sediment record (Lattaud et al., 2018). Alternatively, some mismatches between LDI and $U^{k'}_{37}$ can be explained by the presence of allochtonous input of alkenones (Rosell-Melé et al., 1995; Thomsen et al., 1998; Mollenhauer et al., 2003). This is supported by the observation of Broerse et al. (2000) who find subtropical haptophytes (like *G. oceanica*, *U. sibogae*, and *Coronosphaera* spp.) in sediment traps in the Sea of Okhotsk just after the sea-ice retreated. This suggests that periods of extensive sea-ice coverage in the Sea of Okhotsk are likely to bring alkenones from subtropical regions, possibly due to a change in bottom water circulation. This could bring in resuspended sediment with elevated alkenone concentrations from these subtropical regions, and, combined with low in situ alkenone production, yield higher $U^{k'}_{37}$-SSTs.

The most remarkable feature in the LDI-SST record is the high LDI SST values (around 12 °C) between 1400 and 1200 ka. Although this pattern of higher temperature is also observed in the $U^{k'}_{37}$-SST, it is for a shorter time (1400–1300 ka) and this period has not been recorded as substantially warm in SST records from the north Pacific (Haug et al., 2005; Martinez-Garcia et al., 2010; Kender et al., 2018). Interestingly, this period corresponds to some strong changes in LCD distribution, with a substantial increase in the proportion of the C_{30} 1,15-diol, together with an increase in C_{28} 1,12-diol (up to 14%, data not shown). This unusual distribution and especially the elevated amounts of the C_{28} 1,12-diol potentially points to a different contributor of LCDs which can bias the LDI towards warmer temperatures (De Bar et al., 2019).

As stated above, prior to 1200 ka TEX^{L}_{86}-SWT is lower than $U^{k'}_{37}$ and LDI-SST. Furthermore, during MIS 12 and 16 (ca. 450 and 650 ka, respectively), TEX^{L}_{86}-SWT is relatively low (1.5 ± 1 °C and 3 ± 1 °C respectively, n = 7) in comparison with the other two proxies (5.5 ± 0.5 °C and 8 ± 1 °C for the $U^{k'}_{37}$-SST and 5 ± 0.5 °C and 5 ± 0 °C for LDI-SST, n = 7 for each). Lattaud et al. (2018) showed that the TEX^{L}_{86} is reflecting summer subsurface SWT, potentially explaining the mismatch with LDI and $U^{k'}_{37}$. However, it can also be biased by terrigenous input of GDGTs (Weijers et al., 2009). Examination of

the BIT record shows that it was nearly always below 0.3, suggesting limited riverine input (Weijers et al., 2009). Alternatively, there may have been shifts in season and in depths of production of GDGTs leading to differences between TEX^{L}_{86} and the SST proxies. In the Sea of Okhotsk, due to limited primary productivity during glacials, the source organisms of the GDGTs might also have thrived in spring and autumn due to reduced competition for ammonia (cf. Hurley et al., 2016; Junium et al., 2018) and thus TEX^{L}_{86} would yield lower temperatures. Alternatively, they could be thriving deeper in the water column due to the lower ammonium availability in the surface waters. In a study of the eastern tropical Pacific, Hertzberg et al. (2016) also suggested that TEX_{86} is reconstructing deeper sea water temperature (upper thermocline) during the last glacial maximum due to a deepening of the depth habitat for Thaumarchaeota. Thus, all proxy temperature records seem to be affected by multiple factors such that possibly none of them are reflecting consistently annual mean SST of the Sea of Okhotsk.

4.1.2. Comparison with North Pacific SST records

In contrast to North Pacific SST records (Martinez-Garcia et al., 2010; Horikawa et al., 2015), our Sea of Okhotsk temperature records show no cooling between 1.4 Ma and 1 Ma but rather an increase from 1.3 to 1.1 Ma, in particular with the LDI. However, as discussed above this likely comes from a bias in our temperature proxies. Between 1 and 0.9 Ma, TEX^{L}_{86}-SWT decreases, similar to the northwestern Pacific SST records (site ODP 882, Haug et al., 2005; Martinez-Garcia et al., 2010) and to the Bering Sea SST record (Horikawa et al., 2015). After 0.9 Ma, the northwestern Pacific SST (calculated with $U^{k'}_{37}$ at site ODP 882, Martinez-Garcia et al., 2010) and the Sea of Okhotsk (TEX^{L}_{86}-SWT) are parallel with similar amplitude changes except during MIS 12 and 16, likely due to the deepening of the Thaumarchaeota depth habitat in the Sea of Okhotsk. The last glacial/interglacial transition in the Sea of Okhotsk showed a 10 °C increase but unfortunately site ODP 882 is missing this part and cannot be compared. Thus, in general our TEX^{L}_{86}-SWT records show, despite potential biases, relatively similar patterns in SST as those in the North Pacific as also shown by frequency analysis (see below).

4.1.3. Orbital scale forcing of SSTs

Wavelet analysis of the proxy temperature records shows that the LDI-SST has a significant 100-kyr cycle corresponding to eccentricity (Figs. 4 and S1). The impact of orbital forcing may have been weakened by the changes in season of production of the biomarkers (see above), thereby minimizing SST contrasts between glacial and interglacials. Similarly, the $U^{k'}_{37}$-SST shows only a weak 100-kyr cycle (Fig. 4) and spectral analysis using Redfit (Fig. S1) of the latest 900 ka does not yield any significant periodicity, indicating that the $U^{k'}_{37}$ is possibly impacted by allochtonous input of alkenones. In contrast, the TEX^{L}_{86}-SWT shows a significant 100-kyr cycle and a weak 41-kyr cycle (Fig. S1) linked to eccentricity and obliquity, respectively. Wavelet analysis shows that the 100-kyr periodicity appears after the MPT, i.e. after ~1000 ka, and the 41-kyr is strong before ~1000 ka (Fig. 4c), similar to the LR04 benthic $\delta^{18}O$ stack (Fig. 4f) and $U^{k'}_{37}$-SST record from the northern Pacific (Fig. 4i, Martinez-Garcia et al., 2010). This strongly suggests that TEX^{L}_{86} represents global temperature trends in the Sea of Okhotsk that are (at least partly) orbitally forced, which is also observed in the northern Pacific (Martinez-Garcia et al., 2010). The changes in sea water temperature in the Sea of Okhotsk seems to be linked to ice-sheet extension, i.e. ice albedo, and not local insolation changes as the 23-kyr precession cycle is absent from the spectral analysis, despite that the resolution of our record was sufficient. This would agree with the idea that the northern polar regions are sensitive to planetary albedo forcings (Rohling et al., 2012) and not to dust or greenhouse gases.

4.2. Riverine input and salinity variation

The core site in the central Sea of Okhotsk is in the middle of the basin at 1123 m deep, far removed from the Amur River which is discharging mainly in the eastern part of the basin, bringing with it terrigenous material (Nakatsuka et al., 2004; Seki et al., 2004b and reference cited therein). Indeed, core tops from the central part of the Sea of Okhotsk have a low $F_{C32\ 1,15}$ (0.03–0.12, Table 1) and a low BIT value (0.06–0.1, Table 1). However, in the sediment record these values were at certain times higher than present day (Fig. 3). Furthermore, a significant positive correlation between BIT index and $F_{C32\ 1,15}$ is observed ($r = 0.38$, $p < 0.05$, $n = 395$), in contrast with surface sediments of the Sea of Okhotsk where no correlation is observed (Lattaud et al., 2018). In the oldest part of the record (1500–1200 ka) this relation seems to be absent. The higher values compared to present day, as well as the correlation between BIT and $F_{C32\ 1,15}$, suggest that, in the past, riverine input was more noticeable in the central part of the Sea of Okhotsk. This can be explained by sea-level changes, i.e. during glacial periods the low sea-level (Siddall et al., 2006; Gorbarenko et al., 2014) brought the Amur River mouth closer to the core site, thereby increasing the input of brGDGTs as well as the C_{32} 1,15-diol. A previous study by Lattaud et al. (2017b) in the Mozambique Channel and the eastern Mediterranean showed a similar pattern with elevated BIT index and $F_{C32\ 1,15}$ during sea-level low stands for the late Quaternary. Changes in Amur River input are unlikely to explain the observed patterns as during glacials the Amur River is partially covered by an ice-cap and the amount of terrigenous material reaching the Sea of Okhotsk is reduced (Nürnberg and Tiedemann, 2004). Furthermore, spectral analysis of the $F_{C32\ 1,15}$ record shows that a 100-kyr cycle (linked to eccentricity) initiated after the MPT (Fig. 4, Lisiecki and Raymo, 2005) suggesting a link to changes in sea-level. After 900 ka, a precession cycle (23-kyr) as well as two heterodynes (21- and 19-kyr) are apparent which can be linked to summer insolation (Thomas et al., 2016). The reason for a summer insolation forcing might be that the Asian monsoon is impacted by this forcing and the monsoon system may, in turn, impact the flow of the Amur river system. Before the MPT there is an absence of correlation between the BIT and C_{32} 1,15-diol possibly because glaciations and sea level changes were less severe. Furthermore, there may have been changes in soil sources draining into the Amur River (cf. Lattaud et al., 2017a,b). Since the BIT index represent both soil and river production (De Jonge et al., 2014) and the C_{32} 1,15-diol only comes from rivers, a change in soil source would only impact the BIT but not the C_{32} 1,15-diol.

The δD_{C37} has been shown to reflect past salinity as well as the δD of sea water (Englebrecht and Sachs, 2005; Schouten et al., 2006; Pahnke et al., 2007; van der Meer et al., 2007; Kasper et al., 2014) although other factors such as growth rate can affect this as well (Weiss et al., 2017 and references cited therein). The δD of sea water is controlled, amongst others, by global ice volume and may be affected by input of freshwater from either the Amur River or melting ice. The δD_{C37} record (Fig. 3d) shows a significant negative correlation with the $U^{k'}_{37}$-reconstructed SST ($r^2 = 0.31$, $p < 0.005$, $n = 47$), indicating that warm interglacial stages are characterized by low δD_{C37}. These depleted δD_{C37} values during interglacials are partly linked to the change in ice volume, with a decrease in ice volume leading to a decreased δD of sea water and therefore an decrease in the δD_{C37}. During the transition between MIS 6/5, there is a global increase of 1‰ in $\delta^{18}O_{sea\ water}$ (obtained from Waelbroeck et al., 2002) which corresponds to a global increase in δD_{sea} water of 18‰ (using the global meteoritic water line from Rozanski et al., 1993). However, in the Sea of Okhotsk, the difference in δD_{C37} between glacial and interglacial stages are much higher (up to 30‰, Fig. 3d), and cannot be explained by ice volume alone. Therefore, a substantial part of the change must be due to salinity

changes which changes isotopic fractionation (cf. Kasper et al., 2015). This change in salinity can be due to variations in sea-ice, with increasing sea-ice buildup leading to increased salinity and vice versa, and/or changing freshwater input from the Amur River. Indeed, as discussed above, the Amur River is covered by an ice-cap and its flow into the Sea of Okhotsk is reduced during glacials (Nürnberg and Tiedemann, 2004) leading to increased salinity which would further increase due to extensive sea-ice formation. These combined factors may have led to more saline surface waters during glacials.

4.3. Diatom productivity in the Sea of Okhotsk

The DI (Fig. 3e) and the relative amount of 1,14-diols (Fig. 3f) can be used as qualitative indicators for *Proboscia* diatom productivity. They are both higher at the end of glacial stages (e.g. stages 2/1, 3/2, 6/5, 10/9, 16/15 and during MIS 12). Furthermore, there is also an increase in biogenic opal content which followed the 1,14-diols maxima, indicating that paleoproductivity was higher during deglaciations (Fig. 3). Nürnberg and Tiedemann (2004) also showed an increased productivity during deglaciation in core MD01-2415 from the central Sea of Okhotsk, with biogenic opal content reaching 70% while in our core it reached 60% (Fig. 3g). The biggest increase in biogenic opal happened at the beginning of the Mid-Brunhes Event which is characterized by an increase deep-water dissolution of carbonate all over the world (Jansen et al., 1986; Wang et al., 2003) which in turn increased the opal content in sediments. Biogenic opal in the Sea of Okhotsk is thought to be mainly representing diatoms as other siliceous organisms are less abundant in the Sea of Okhotsk (Iwasaki et al., 2012). However, since *Proboscia* diatoms have a weak silicified shell which are easily dissolved (Haake et al., 1993; Sakka et al., 1999; Koning et al., 2001; Rampen et al., 2011), they likely do not contribute substantially to the opal content. The succession of an opal maximum after a 1,14-diols maximum is likely due to the competition between *Proboscia* diatoms and other, more heavily silicified diatoms (like *Chaetoceros* in the modern Sea of Okhotsk, Tsoy et al., 2009; Riegman, 1995; Riegman et al., 1996) that will outcompete the *Proboscia* when silica is not limiting (Riegman et al., 1996; Ragueneau et al., 2006; Zhu et al., 2018). The increases in DI followed by increased in opal content is also observed in an offshore core from the Peru upwelling margin (De Bar et al., 2018) but, in contrast to the Peru margin, there is no systematic upwelling in the Sea of Okhotsk. Here, the presence of *Proboscia* is more likely linked to nutrient availability as noticed by Willmott et al. (2010) for coastal Antarctica. The wavelet analysis shows for the opal content and 1,14-diols a 100-kyr cycle, linked to eccentricity, after the MPT, suggesting that diatom productivity is impacted by glacial/interglacial changes which impacts sea level and nutrient availability. This is in agreement with the idea that primary productivity in the Sea of Okhotsk is regulated by the progress and retreat of sea-ice (Nürnberg and Tiedemann, 2004; Seki et al., 2004b; Iwasaki et al., 2012; Bosin et al., 2015) with the retreat and melting of sea-ice providing more light for algal blooming, increased vertical mixing supplying silica to the surface layer and enhanced silica input by the Amur River.

The heterodyne-rich spectrum of the productivity proxies indicate multiple environmental forcing mechanisms. Some periods such as ~34-kyr (related to precession and eccentricity, Fig. S1) in the 1,14-diol record can be explained by the influence of the Amur River and the input of cold nutrient-rich water that enhance diatom productivity (Wang et al., 2008). Indeed the volume of terrigenous material from the Amur River discharging into the Sea of Okhotsk is partly controlled by the Asian monsoon (Harada et al., 2008) which is, in turn, mainly controlled by precession and summer insolation (Thomas et al., 2016). Similarly, the biogenic opal percentage also show clear precession bands. (23-kyr, Fig. S1) indicating that primary productivity in the Sea of Okhotsk is primarily controlled by the progress and retreat of sea-ice but also by the amount of riverine input into the Sea.

During MIS 29-21 (1020–840 ka), the Bering Sea (also a North Pacific marginal sea like the Sea of Okhotsk) showed a decrease in primary productivity (mainly diatoms, Kanematsu et al., 2013; Detlef et al., 2018; Kender et al., 2018), which is similar to what happened in the northwestern Pacific (site ODP 882, Martinez-Garcia et al., 2010). This decrease in productivity might be due to limited nutrient availability (reduction of iron fertilization via river input and shelf remobilization), light limitation, and reduced glacial upwelling of nutrients (Kender et al., 2018). During that time period the Sea of Okhotsk only had limited exchange with the North Pacific due to the low sea-level (St. John and Krissek, 1999) and diatom productivity decreased before the MPT (1400–1250 ka) but remained high between 1020 and 840 ka, as also observed by Nürnberg and Tiedemann (2004) which might be due to the constant input of iron to the Sea of Okhotsk (Nishioka et al., 2007; Ohshima et al., 2014).

5. Conclusions

In this study we analyzed a variety of long-chain diol proxies in a 1.5 Ma sediment core from the central Sea of Okhotsk. The LDI-SST seems to represent autumn SST during interglacials and possibly summer SST during glacials. In contrast, TEX^{L}_{86} seems to represent summer subsurface SWT during most of the time although sometimes also deeper water depths during glacial periods. The LDI-SST and $U^{k'}_{37}$ do not show any obvious and persistent periodicity, while the TEX^{L}_{86} has a dominant 100-kyr cycle appearing after the MPT. The lack of periodicity in the LDI and $U^{k'}_{37}$ is likely due to seasonal bias in the LDI and input of lateral transported alkenones for the $U^{k'}_{37}$.

The DI, the relative abundance of 1,14-diols and opal content in the sediment are all elevated during deglaciations and show a 100-kyr cyclicity in their records after the MPT. The recurrent lag between maxima of 1,14-diols and opal content suggests a competition for silica availability between *Proboscia* diatoms and heavily silica-shelled diatoms (recorded via the biogenic opal content of the sediment). The $F_{C32\ 1,15}$ as a proxy for river input is mainly linked with sea-level variation as it shows a 100-kyr cyclicity after the MPT. This is likely because during lower sea-level stands, i.e. during glacials, more riverine C_{32} 1,15-diol will be brought to the core site than during interglacials. In conclusion, this study shows that proxies based on long chain diols can be of use to reveal long term paleoceanographic changes in subpolar oceans.

Conflict of interest

The authors declare that they have no conflict of interest.

Acknowledgments

We thank two anonymous reviewers and the associate editor I. Castañeda for their useful comments on this manuscript. We thank Denise Dorhout, Jort Ossebaar and Anchelique Mets for technical assistance and Rick Hennekam for discussion on the spectral analysis. This research has been funded by the European Research Council (ERC) under the European Union's Seventh Framework Program (FP7/2007-2013) ERC grant agreement [339206] to S.S. The work was further supported by funding from the Netherlands Earth System Science Center (NESSC) through a gravitation grant (NWO 024.002.001) from the Dutch Ministry for Education, Culture and Science to JSSD and SS. L.L. was supported by grants of

National Natural Science Foundation of China (41773116), State Key Laboratory of Isotope Geochemistry, Guangzhou Institute of Geochemistry, Chinese Academy of Sciences start-up fund and 135 project (SKLaBIG-QD- 16-04 and 135PY201605) and the Ministry of Science and Technology (MOST), Taiwan ROC (104-2917-I-564-046). Samples of core MD01-2414 were generously provided by Taiwan Ocean Research Institute (TORI). Data are available at Pangaea (doi: https://doi.org/10.1594/PANGAEA.896775).

Appendix A. Supplementary material

Supplementary data to this article can be found online at https://doi.org/10.1016/j.orggeochem.2019.04.003.

Associate Editor—**Isla S. Castaneda**

References

Antonov, J.I., Seidov, D., Boyer, T.P., Locarnini, R.A., Mishonov, A.V., Garcia, H.E., 2010. World Ocean Atlas 2009, Volume 2: Salinity. In: Levitus, S. (Ed.), NOAA Atlas NESDIS 69. U.S. Government Printing Office, Washington, D.C., 184 pp. URL: ftp://ftp.nodc.noaa.gov/pub/WOA09/DOC/woa09_vol2_text.pdf.

Berger, A., Li, X.S., Loutre, M.F., 1999. Modelling northern hemisphere ice volume over the last 3 Ma. Quaternary Science Reviews 18 (1), 1–11. https://doi.org/10.1016/S0277-3791(98)00033-X.

Bosin, A., Gorbarenko, S., Xuefa, S., Liu, Y., Zou, J., 2015. Regionalized primary paleoproduction variability in the Sea of Okhotsk during late Pleistocene and Holocene. Journal of Asian Earth Science 114, 534–540. https://doi.org/10.1016/j.jseaes.2015.07.019.

Broerse, A.T.C., Ziveri, P., Honjo, S., 2000. Coccolithophore ($-CaCO_3$) flux in the Sea of Okhotsk seasonality, settling and alteration processes. Marine Micropaleontology 39, 179–200. https://doi.org/10.1016/S0377-8398(00)00020-7.

Chou, Y., Lee, T., Song, S., Chen, K., 2011. Magnetostratigraphy of marine sediment core MD01-2414 from Okhotsk Sea and its paleoenvironmental implications. Marine Geology 284, 149–157. https://doi.org/10.1016/j.margeo.2011.03.015.

Clark, P.U., Pollard, D., 1998. Origin of the Middle Pleistocene transition by ice sheet erosion of regolith. Paleoceanography 13, 1–9. https://doi.org/10.1029/97PA02660.

Clark, P.U., Archer, D., Pollard, D., Blum, J.D., Rial, J.A., Brovkin, V., Mix, A.C., Pisias, N.G., Roy, M., 2006. The middle Pleistocene transition: characteristics, mechanisms, and implications for long-term changes in atmospheric pCO2. Quaternary Science Reviews 25 (23–24), 3150–3184. https://doi.org/10.1016/j.quascirev.2006.07.008.

De Bar, M.W., Dorhout, D.J.C., Hopmans, E.C., Sinninghe Damsté, J.S., Schouten, S., 2016. Constraints on the application of long chain diol proxies in the Iberian Atlantic margin. Organic Geochemistry 184–195. https://doi.org/10.1016/j.orggeochem.2016.09.005.

De Bar, M.W., Stolwijk, D.J., McManus, J.F., Sinninghe Damsté, J.S., Schouten, S., 2018. A late Quaternary climate record based on long chain diol proxies from the Chilean margin. Climate of the Past 14, 1783–1803. https://doi.org/10.5194/cp-14-1783-2018.

De Bar, M.W., Rampen, S.W., Hopmans, E.C., Damsté, J.S.S., Schouten, S., 2019. Constraining the applicability of organic paleotemperature proxies for the last 90 Myrs. Organic Geochemistry 128, 122–136. https://doi.org/10.1016/j.orggeochem.2018.12.005.

De Jonge, C., Stadnitskaia, A., Hopmans, E.C., Cherkashov, G., Fedotov, A., Sinninghe Damsté, J.S., 2014. In situ produced branched glycerol dialkyl glycerol tetraethers in suspended particulate matter from the Yenisei River, Eastern Siberia. Geochimica and Cosmochimica Acta 125, 476–491. https://doi.org/10.1016/j.gca.2013.10.031.

Detlef, H., Belt, S.T., Sosdian, S.M., Smik, L., Lear, C.H., Hall, I.R., Cabedo-Sanz, P., Husum, K., Kender, S., 2018. Sea ice dynamics across the Mid-Pleistocene transition in the Bering Sea. Nature Communications 9 (1), 941. https://doi.org/10.1038/s41467-018-02845-5.

Elderfield, H., Ferretti, P., Greaves, M., Crowhurst, S., McCave, I.N., Hodell, D.A., Piotrowski, A.M., 2012. Evolution of ocean temperature and ice volume through the mid-Pleistocene climate transition. Science 337 (6095), 704–709. https://doi.org/10.1126/science.1221294.

Englebrecht, A.C., Sachs, J.P., 2005. Determination of sediment provenance at drift sites using hydrogen isotopes and unsaturation ratios in alkenones. Geochimica et Cosmochimica Acta 69 (17), 4253–4265. https://doi.org/10.1016/j.gca.2005.04.011.

Gorbarenko, S.A., 1996. Stable isotope and lithologic evidence of late-glacial and holocene oceanography of the northwestern pacific and its marginal seas. Quaternary Research 46, 230–250. https://doi.org/10.1006/qres.1996.0063.

Gorbarenko, S.A., Southon, J.R., Keigwin, L.D., Cherepanova, M.V., Gvozdeva, I.G., 2004. Late Pleistocene-Holocene oceanographic variability in the Okhotsk Sea: geochemical, lithological and paleontological evidence. Paleogeography, Paleoclimatoogy, Paleoecology 209, 281–301. https://doi.org/10.1016/j.palaeo.2004.02.013.

Gorbarenko, S.A., L'vovich Goldberg, E., Kashgaria, M., Velivetskaya, T.A., Zakharkov, S.P., Pechnikov, V.S., Bosin, A.A., Psheneva, O.Y., Ivanova, E.D., 2007. Millennium scale environment changes of the Okhotsk Sea during Last 80 kyr and their phase relationship with global climate changes. Journal of Oceanography 63, 609–623. https://doi.org/10.1007/s10872-007-0054-1.

Gorbarenko, S.A., Harada, N., Malakhov, M.I., Vasilenko, Y.P., Bosin, A.A., Goldberg, E.L., 2010. Orbital and millennial-scale environmental and sedimentological changes in the Okhotsk Sea during the last 350 kyr. Global and Planetary Changes 72, 79–85. https://doi.org/10.1016/j.gloplacha.2010.03.002.

Gorbarenko, S.A., Harada, N., Malakhov, M.I., Velivetskaya, T.A., Vasilenko, Y.P., Bosin, A.A., Derkachev, A.N., Goldberg, E.L., Ignatiev, A.V., 2012. Responses of the Okhotsk Sea environment and sedimentology to global climate changes at the orbital and millennial scale during the last 350kyr. Deep Sea Research II 61–64, 73–84. https://doi.org/10.1016/j.dsr2.2011.05.016.

Gorbarenko, S.A., Artemova, A.V., Goldberg, E.L., Vasilenko, Y.P., 2014. The response of the Okhotsk Sea environment to the orbital-millennium global climate changes during the Last Glacial Maximum, deglaciation and Holocene. Global and Planetary Changes 116, 76–90. https://doi.org/10.1016/j.gloplacha.2014.02.002.

Haake, B., Ittekkot, V., Rixen, T., Ramaswamy, V., Nair, R.R., Curry, W.B., 1993. Seasonality and interannual variability of particle fluxes to the deep Arabian Sea. Deep Sea Research Part I: Oceanographic Research Papers 40, 1323–1344. https://doi.org/10.1016/0967-0637(93)90114-I.

Hammer, Ø., Harper, D.A.T., Ryan, P.D., 2001. PAST: Paleontological statistics software package for education and data analysis 9 Palaeontologia Electronica 4 (1) http://palaeo-electronica.org/2001_1/past/issue1_01.htm.

Harada, N., Ahagon, N., Uchida, M., Murayama, M., 2004. Northward and southward migrations of frontal zones during the past 40 kyr in the Kuroshio-Oyashio transition area. Geochemistry, Geophysics, Geosystems 5 (9), Q09004. https://doi.org/10.1029/2004GC000740.

Harada, N., Ahagon, N., Sakamoro, T., Uchida, M., Ikhehara, M., Shibata, Y., 2006. Rapid fluctuation of alkenone temperature in the southwestern Okhotsk Sea during the past 120 ky. Global and Planetary Changes 53, 29–46. https://doi.org/10.1016/j.gloplacha.2006.01.010.

Harada, N., Sato, M., Sakamoto, T., 2008. Freshwater impacts recorded in tetraunsaturated alkenones and alkenone sea surface temperatures from the Okhotsk Sea across millennial-scale cycles. Paleoceanography and Paleoclimatology. 23, PA3201. https://doi.org/10.1029/2006PA001410.

Harada, N., Sato, M., Seki, O., Timmermann, A., Moossen, H., Bendle, J., Nakalura, Y., Kimoto, K., Okazaki, Y., Nagashima, K., Gorbarenko, S.A., Ijiri, A., Kakatsuka, T., Menviel, L., Chikamoto, M.O., Abe-Ouchi, A., Schouten, S., 2012. Sea surface temperature changes in the Okhotsk Sea and adjacent North Pacific during the last glacial maximum and deglaciation. Deep Sea Research II 61–64, 93–105. https://doi.org/10.1016/j.dsr2.2011.12.007.

Harada, N., Katsuki, K., Nakagawa, M., Matsumoto, A., Seki, O., Addison, J., Finney, B.P., Sato, M., 2014. Holocene sea surface temperature and sea ice extent in the Okhotsk and Bering Seas. Progress in Oceanography 126, 242–253. https://doi.org/10.1016/j.pocean.2014.04.017.

Haug, G.H., Ganopolski, A., Sigman, D.M., Rosell-Mele, A., Swann, G.E., Tiedemann, R., Jaccard, S.L., Bollmann, J., Maslin, M.A., Leng, M.J., Eglinton, G., 2005. North Pacific seasonality and the glaciation of North America 2.7 million years ago. Nature 433 (7028), 821–825. https://doi.org/10.1038/nature03332.

Hays, J.D., Imbrie, J., Shackleton, N.J., 1976. Variations in the Earth's orbit: pacemaker of the ice ages. Science 194, 1121–1132. https://doi.org/10.1126/science.194.4270.1121.

Hays, J.D., Morlet, J.J., 2003. The sea of Okhotsk a window on the Ice Age Ocean. Deep Sea Research I 50, 1481–1506. https://doi.org/10.1016/j.dsr.2003.08.002.

Hertzberg, J.E., Schmidt, M.W., Bianchi, T.S., Smith, R.W., Shields, M.R., Marcantonio, F., 2016. Comparison of eastern tropical Pacific TEX86 and Globigerinoides ruber Mg/Ca derived sea surface temperatures: insights from the Holocene and Last Glacial Maximum. Earth and Planetary Science Letters 434, 320–332. https://doi.org/10.1016/j.epsl.2015.11.050.

Hopmans, E., Weijers, J., Schefuß, E., Herfort, L., Sinninghe Damste, J.S., Schouten, S., 2004. A novel proxy for terrestrial organic matter in sediments based on branched and isoprenoid tetraether lipids. Earth and Planetary Science Letter 224, 107–116. https://doi.org/10.1016/j.epsl.2004.05.012.

Horikawa, K., Martin, E.E., Basak, C., Onodera, J., Seki, O., Sakamoto, T., Ikehara, M., Sakai, S., Kawamura, K., 2015. Pliocene cooling enhanced by flow of low-salinity Bering Sea water to the Arctic Ocean. Nature Communications 6, 7587. https://doi.org/10.1038/ncomms8587.

Hurley, S.J., Elling, F.J., Könneke, M., Buchwald, C., Wankel, S.D., Santoro, A.E., Lipp, J.S., Hinrich, K.-U., Pearson, A., 2016. Influence of ammonia oxidation rate on thaumarchaeal lipid composition and the TEX86 temperature proxy. Proceedings of the National Academy of Sciences 113 (28), 7762–7767. https://doi.org/10.1073/pnas.1518534113.

Ishawatari, R., Fujino, N., Brincat, D., Yamamoto, S., Takahara, H., Shichi, K., Krivonogov, S.K., 2009. A 35kyr record of organic matter composition of δ13C of n-alkane in bog sediments close to lake Baikal implications for paleoenvironmental studies. Organic Geochemistry 40, 51–60. https://doi.org/10.1016/j.orggeochem.2008.09.007.

Iwasaki, S., Takahashi, K., Maesawa, T., Sakamoto, T., Sakai, S., Iijima, K., 2012. Paleoceanography of the last 500 kyrs in the central Okhotsk Sea based on geochemistry. Deep-Sea Research II. 61–64, 50–62. https://doi.org/10.1016/j.dsr2.2011.03.003.

Jansen, J.H.F., Kuijpers, A., Troelstra, S.R., 1986. A mid-Brunhes climatic event: long-term changes in global atmosphere and ocean circulation. Science 232 (4750), 619–622. https://doi.org/10.1126/science.232.4750.619.

Jonas, A.S., Schwark, L., Bauersachs, T., 2017. Late Quaternary water temperature variations of the Northwest Pacific based on lipid paleothermometers TEXH86, $U^{k'}_{37}$ and LDI. Deep Sea Research Part I. https://doi.org/10.1016/j.dsr.2017.04.018. DSRI2791.

Junium, C.K., Meyers, S.R., Arthur, M.A., 2018. Nitrogen cycle dynamics in the Late Cretaceous Greenhouse. Earth and Planetary Science Letters 481, 404–411. https://doi.org/10.1016/j.epsl.2017.10.006.

Kanematsu, Y., Takahashi, K., Kim, S., Asahi, H., Khim, B.K., 2013. Changes in biogenic opal productivity with Milankovitch cycles during the last 1.3 Ma at IODP Expedition 323 Sites U1341, U1343, and U1345 in the Bering Sea. Quaternary International 310, 213–220. https://doi.org/10.1016/j.quaint.2013.06.003.

Kasper, S., Van Der Meer, M.T.J., Mets, A., Zahn, R., Sinninghe Damsté, J.S., Schouten, S., 2014. Salinity changes in the Agulhas leakage area recorded by stable hydrogen isotopes of C 37 alkenones during Termination I and II. Climate of the Past 10 (1), 251–260. https://doi.org/10.5194/cp-10-251-2014.

Kasper, S., van der Meer, M., Castaneda, I., Tjallingii, R., Brummer, G.-J., Sinninghe Damsté, J.S., Schouten, S., 2015. Testing the alkenone D/H ratio as a paleo indicator of sea surface salinity in a coastal ocean margin (Mozambique Channel). Organic Geochemistry 78, 62–68. https://doi.org/10.1016/j.orggeochem.2014.10.011.

Katsuki, K., Khim, B.-K., Itaki, T., Okazaki, Y., Ikehara, K., Shin, Y., Yoon, H.I., Kang, C. Y., 2010. Sea-ice distribution and atmospheric pressure patterns in southwestern Okhotsk Sea since the Last Glacial Maximum. Global and Planetary Change 72, 99–107. https://doi.org/10.1016/j.gloplacha.2009.12.005.

Kender, S., Ravelo, A.C., Worne, S., Swann, G.E., Leng, M.J., Asahi, H., Becker, J., Detlef, H., Aiello, I.W., Andreasen, D., Hall, I.R., 2018. Closure of the bering strait caused mid-pleistocene transition cooling. Nature Communications 9. https://doi.org/10.1038/s41467-018-07828-0.

Khim, B.K., Sakamoto, T., Harada, N., 2012. Reconstruction of surface water conditions in the central region of the Okhotsk Sea during the last 180 kyrs. Deep Sea Research Part II: Topical Studies in Oceanography 61, 63–72. https://doi.org/10.1016/j.dsr2.2011.05.014.

Kim, J.-H., van der Meer, M., Schouten, S., Helmke, P., Willmott, V., Sangiorgi, F., Koc, N., Hopmans, E.C., Sinninghe Damsté, J.S., 2010. New indices and calibrations derived from the distribution of crenarchaeol isoprenoid tetraether lipids: implication for past sea surface temperature reconstructions. Geochemica and Cosmochimica Acta. 74, 4639–4654. https://doi.org/10.1016/j.gca.2010.05.027.

Koning, E., van Iperen, J.M., van Raaphorst, W., Helder, W., Brummer, G.J.A., van Weering, T.C.E., 2001. Selective preservation of upwelling-indicating diatoms in sediments off Somalia, NW Indian Ocean. Deep Sea Research Part I: Oceanography 48, 2473–2495. https://doi.org/10.1016/S0967-0637(01)00019-X.

Kotthoff, U., Groeneveld, J., Ash, J.L., Fanget, A.S., Krupinski, N.Q., Peyron, O., Stepanova, A., Warnock, J., Van Helmond, N.A., Passey, B.H., Clausen, O.R., 2017. Reconstructing Holocene temperature and salinity variations in the western Baltic Sea region: a multi-proxy comparison from the Little Belt (IODP Expedition 347, Site M0059). Biogeosciences 14 (23), 5607. https://doi.org/10.5194/bg-14-5607-2017.

Lattaud, J., Kim, J.-H., De Jonge, C., Zell, C., Sinninghe Damsté, J.S., Schouten, S., 2017a. The C32 alkane-1,15-diol as a tracer for riverine input in coastal seas. Geochimica and Cosmochimica Acta 202 (146–158). https://doi.org/10.1016/j.gca.2016.12.030.

Lattaud, J., Dorhout, D., Schulz, H., Castañeda, I.C., Schefuß, E., Sinninghe Damsté, J. S., Schouten, S., 2017b. The C32 alkane-1,15-diol as a proxy for late Quaternary riverine input in coastal margins. Climate of the Past 13, 1049–1061. https://doi.org/10.5194/cp-13-1049-2017.

Lattaud, J., Lo, L., Huang, J.-J., Chou, Y.-M., Gorbarenko, S.A., Sinninghe Damsté, J.S., Schouten, S., 2018. A comparison of Late Quaternary paleotemperature records of the central Okhotsk Sea based on organic proxies. Paleoceanography and Paleoclimatology. https://doi.org/10.1029/2018PA003388.

Lembke-Jene, L., Tiedemann, R., Nürnberg, D., Gong, X., Lohmann, G., 2018. Rapid shift and millennial-scale variations in Holocene North Pacific Intermediate Water ventilation. Proceedings of the National Academy of Sciences. https://doi.org/10.1073/pnas.1714754115.

Lisiecki, L., Raymo, M., 2005. A Pliocene-Pleistocene stack of 57 globally distributed benthic δ18O records. Paleoceanography 20, 1003–1020. https://doi.org/10.1029/2004PA001071.

Liu, Y.-J., Song, S.-R., Lee, T.-Q., Lee, M.-Y., Chen, Y.-L., Chen, H.-F., 2006. Mineralogical and geochemical changes in the sediments of the Okhotsk Sea during deglacial periods in the past 500 kyrs. Global and Planetary Change 53, 47–57. https://doi.org/10.1016/j.gloplacha.2006.01.007.

Lo, L., Belt, S., Lattaud, J., Friedrich, T., Zeeden, C., Schouten, S., Smik, L., Timmermann, A., Cabedo-Sanz, P., Huand, J.-J., Zhou, L., Ou, T.-H., Chang, Y.-P., Wang, L.-C., Chou, Y.-M., Shen, C.-C., Chen, M.-T., Wei, K.-Y., Son, S.-R., Fang, T.-H., Gorbarenko, S.A., Wang, W.-L., Lee, T.-Q., Elderfield, H., Hodell, D.A., 2018. Precession and atmospheric CO2 modulated variability of sea ice in the central Okhotsk Sea since 130,000 years ago. Earth and Planetary Science Letter 488, 36–45. https://doi.org/10.1016/j.epsl.2018.02.005.

Locarnini, R.A., Mishonov, A.V., Antonov, J.I., Boyer, T.P., Garcia, H.E., 2010. World Ocean Atlas 2009, Volume 1: Temperature. In: Levitus, S. (Ed.), NOAA Atlas NESDIS 68. U.S. Government Printing Office, Washington, D.C., 184 pp. URL: ftp://ftp.nodc.noaa.gov/pub/WOA09/DOC/woa09_vol1_text.pdf.

Lopes dos Santos, R.A.L., Wilkins, D., De Deckker, P., Schouten, S., 2012. Late Quaternary productivity changes from offshore Southeastern Australia: a biomarker approach. Palaeogeography, Palaeoclimatology, Palaeoecology 363, 48–56. https://doi.org/10.1016/j.palaeo.2012.08.013.

Malakhov, M.I., Gorbarenko, S.A., Malakhova, G.Y., Harada, N., Vasilenko, Y.P., Bosin, A.A., Goldberg, E.L., Derkachev, A.N., 2009. Petromagnetic parameters of bottom sediments as indicators of the climatic and environmental changes in the central zone of the Sea of Okhotsk during the last 350 kyr. Russian Geology and Geophysics 50, 973–982. https://doi.org/10.1016/j.rgg.2009.10.006.

Martínez-Garcia, A., Rosell-Melé, A., McClymont, E.L., Gersonde, R., Haug, G.H., 2010. Subpolar link to the emergence of the modern equatorial Pacific cold tongue. Science 328 (5985), 1550–1553.

Medina-Elizalde, M., Lea, D.W., 2005. The Mid-Pleistocene transition in the tropical pacific. Science 310, 1009–1012. https://doi.org/10.1126/science.1115933.

McClymont, E.L., Rosell-Melé, A., Haug, G.H., Lloyd, J.M., 2008. Expansion of subarctic water masses in the North Atlantic and Pacific oceans and implications for mid-Pleistocene ice sheet growth. Paleoceanography 23, PA4214. https://doi.org/10.1029/2008PA001622.

McClymont, E.L., Sosdian, S., Rosell-Melé, A., Rosenthal, Y., 2013. Pleistocene sea-surface temperature evolution: early cooling, delayed glacial intensification, and implications for the mid-Pleistocene climate transition. Earth-Science Review 123, 173–193. https://doi.org/10.1016/j.earscirev.2013.04.006.

Mollenhauer, G., Eglinton, T.I., Ohkouchi, N., Schneider, R.R., Müller, P.J., Grootes, P. M., Rullkötter, J., 2003. Asynchronous alkenone and foraminifera records from the Benguela Upwelling System. Geochimica and Cosmochimica Acta 67 (12), 2157–2171. https://doi.org/10.1016/S0016-7037(03)00168-6.

Nakanowatari, T., Nakamura, T., Uchimoto, K., Uehara, H., Mitsudera, H., Ohshima, K. I., Hasumo, H., Wakatsuchi, M., 2014. Causes of the multidecadal-scale warming of the intermediate water in the Okhotsk Sea and Western Subarctic North Pacific. Journal of Climate 28. https://doi.org/10.1175/JCLI-D-14-00172.1.

Nakatsuka, T., Toda, M., Kawamura, K., Wakatsuchi, M., 2004. Dissolved and particulate organic carbon in the Sea of Okhotsk: transport from continental shelf to ocean interior. Journal of Geophysical Research: Oceans 109 (C9). https://doi.org/10.1029/2003JC001909.

Nishioka, J., Ono, T., Saito, H., Nakatsuka, T., Takeda, S., Yoshimura, T., Suzuki, K., Kuma, K., Nakabayashi, S., Tsumune, D., Mitsudera, H., Johnson, W.K., Tsuda, A., 2007. Iron supply to the western subarctic Pacific: importance of iron export from the Sea of Okhotsk. Journal of Geophysical Research 112, C10012. https://doi.org/10.1029/2006JC004055.

Nürnberg, D., Tiedemann, R., 2004. Environmental change in the Sea of Okhotsk during the last 1.1 million years. Paleoceanography 19 (4). https://doi.org/10.1029/2004PA001023.

Nürnberg, D., Dethleff, D., Tiedemann, R., Kaiser, A., Gorbarenko, S., 2011. Okhotsk Sea ice coverage and Kamchatka glaciation over the last 350 ka-evidence from ice-rafted debris and planktonic δ18O. Palaeogeography, Palaeoclimatology, Palaeoecology 310, 191–205. https://doi.org/10.1016/j.palaeo.2011.07.011.

Ohshima, K.I., Nakanowatari, T., Riser, S., Volkov, Y., Wakatsuchi, M., 2014. Freshening and dense shelf water reduction in the Okhotsk Sea linked with sea ice decline. Progress in Oceanography 126, 71–79. https://doi.org/10.1016/j.pocean.2014.04.020.

Pahnke, K., Sachs, J.P., Keigwin, L., Timmermann, A., Xie, S.P., 2007. Eastern tropical Pacific hydrologic changes during the past 27,000 years from D/H ratios in alkenones. Paleoceanography 22 (4). https://doi.org/10.1029/2007PA001468.

Pisias, N.G., Moore Jr, T.C., 1981. The evolution of the Pleistocene climate: a time series approach. Earth and Planetary Science Letters 52, 450–458. https://doi.org/10.1016/0012-821X(81)90197-7.

Plancq, J., Grossi, V., Pittet, B., Huguet, C., Rosell-Melé, A., Mattioli, E., 2015. Multi-proxy constraints on sapropel formation during the late Pliocene of central Mediterranean (southwest Sicily). Earth and Planetary Science Letters 420, 30–44. https://doi.org/10.1016/j.epsl.2015.03.031.

Prahl, F., Wakeham, S.G., 1987. Calibration of unsaturation patterns in long-chain ketone compositions for palaeotemperature assessment. Nature 330, 367–369. https://doi.org/10.1038/330367a0.

Ragueneau, O., Schultes, S., Bidle, K., Claquin, P., Moriceau, B., 2006. Si and C interactions in the world ocean: Importance of ecological processes and implications for the role of diatoms in the biological pump. Global Biogeochemical Cycles 20, GB4S02. https://doi.org/10.1029/2006GB002688.

Rampen, S.W., Schouten, S., Wakeham, S.G., Sinninghe Damsté, J.S., 2007. Seasonal and spatial variation in the sources and fluxes of long chain diols and mid-chain hydroxy methyl alkanoates in the Arabian Sea. Organic Geochemistry 38, 165–179.

Rampen, S.W., Schouten, S., Sinninghe Damsté, J.S., 2011. Occurrence of long chain 1,14-diols in Apedinella radians. Organic Geochemistry 42, 572–574. https://doi.org/10.1016/j.orggeochem.2011.03.009.

Rampen, S.W., Willmott, V., Kim, J.-H., Uliana, E., Mollenhauer, G., Schefuß, E., Sinninghe Damsté, J.S., Schouten, S., 2012. Long chain 1,13- and 1,15-diols as a potential proxy for palaeotemperature reconstruction. Geochimica and Cosmochimica Acta 84, 204–216. https://doi.org/10.1016/j.gca.2012.01.024.

Rampen, S.W., Willmott, V., Kim, J.-H., Rodrigo-Gamiz, M., Uliana, E., Mollenhauer, G., Schefuss, E., Sinninghe Damsté, J.S., Schouten, S., 2014. Evaluation of long chain 1,14-alkyl diols in marine sediments as indicators for upwelling and temperature. Organic Geochemistry 76, 39–47. https://doi.org/10.1016/j.orggeochem.2014.07.012.

Raymo, M.E., Ruddiman, W.F., Shackelton, N.J., Oppo, D.W., 1990. Evolution of Atlantic-Pacific δ13C gradients over the last 2.5 m.y. Earth and Planetary Science Letter 97, 353–368. https://doi.org/10.1016/0012-821X(90)90051-X.

Riegman, R., 1995. Nutrient-related selection mechanisms in marine phytoplankton communities and the impact of eutrophication on the planktonic food web. Water Science and Technology 32 (4), 63–75. https://doi.org/10.1016/0273-1223(95)00682-6.

Riegman, R., De Boer, M., de Senerpont Domis, L., 1996. Growth of harmful marine algae in multispecies cultures. Journal of Planktonic Research 18 (10), 1851–1866. https://doi.org/10.1093/plankt/18.10.1851.

Rodrigo-Gamiz, M., Rampen, S.W., de Haas, H., Baas, M., Schouten, S., Sinninghe Damsté, J.S., 2015. Constraints on the applicability of the organic temperature proxies UK'37, TEX86 and LDI in the subpolar region around Iceland. Biogeoscienes 12, 6573–6590. https://doi.org/10.5194/bg-12-6573-2015.

Rosell-Melé, A., Eglinton, G., Pflaumann, U., Sarnthein, M., 1995. Atlantic core-top calibration of the U37K index as a sea-surface palaeotemperature indicator. Geochimica and Cosmochimica Acta 59 (15), 3099–3107. https://doi.org/10.1016/0016-7037(95)00199-A.

Rozanski, K., Araguás-Araguás, L., Gonfiantini, R., 1993. Isotopic patterns in modern global precipitation. Climate Change in Continental Isotopic Records 78, 1–36. https://doi.org/10.1029/GM078p0001.

Rohling, E.J., Medina-Elizalde, M., Shepherd, J.G., Siddall, M., Stanford, J.D., 2012. Sea surface and high-latitude temperature sensitivity to radiative forcing of climate over several glacial cycles. Journal of Climate 25 (5), 1635–1656.

Sakamoto, T., Ikehara, M., Aoki, K., Iijima, K., Kimura, N., Nakatsuka, T., Wakatsuchi, M., 2005. Ice-rafted debris (IRD)-based sea-ice expansion events during the past 100 kyrs in the Okhotsk Sea. Deep Sea Research Part II: Topical Studies in Oceanography 52 (16–18), 2275–2301. https://doi.org/10.1016/j.dsr2.2005.08.007.

Sakamoto, T., Ikehara, M., Uchida, M., Aoki, K., Shibata, Y., Kanamatsu, T., Harada, N., Ijima, K., Katsuki, K., Asahi, H., Takahashi, K., Sakai, H., Kawahata, H., 2006. Millennial-scale variations of sea-ice expansion in the southwestern part of the Okhotsk Sea during the past 120 kyr: Age model and ice-rafted debris in IMAGES Core MD01-2412. Global and Planetary Change 53 (1–2), 58–77. https://doi.org/10.1016/j.gloplacha.2006.01.012.

Sakka, A., Legendre, L., Gosselin, M., Leblanc, B., Delesalle, B., Price, N., 1999. Nitrate, phosphate, and iron limitation of the phytoplankton assemblage in the lagoon of Takapoto Atoll (Tuamotu Archipelago, French Polynesia). Aquatic Microbial Ecology 19, 149–161. https://doi.org/10.3354/ame019149.

Schefuß, E., Sinninghe Damsté, J.S., Jansen, J.H.F., 2004. Forcing of tropical Atlantic sea surface temperatures during the mid-Pleistocene transition. Paleoceanography 19, PA4029. https://doi.org/10.1029/2003PA000892.

Schouten, S., Ossebaar, J., Schreiber, K., Kienhuis, M.V.M., Langer, G., Benthien, A., Bijma, J., 2006. The effect of temperature, salinity and growth rate on the stable hydrogen isotopic composition of long chain alkenones produced by Emiliania huxleyi and Gephyrocapsa oceanica. Biogeosciences 3, 113–119. https://doi.org/10.5194/bg-3-113-2006.

Seki, O., Kawamura, K., Ikehara, M., Nakatsuka, T., Oba, T., 2004a. Variation of alkenone sea surface temperature in the Sea of Okhotsk over the last 85 kyrs. Organic Geochemistry 35, 347–354. https://doi.org/10.1016/j.orggeochem.2003.10.011.

Seki, O., Ikhehara, M., Kawamura, K., Nakatsuka, T., Ohnishi, K., Narita, H., Sakamoto, T., 2004b. Reconstruction of paleoproductivity in the Sea of Okhotsk over the last 30 kyr. Paleoceanography and Paleoclimatology 19 (1). https://doi.org/10.1029/2002PA000808.

Seki, O., Sakamoto, T., Sakai, S., Schouten, S., Hopmans, E.C., Sinninghe Damsté, J.S., 2009. Large changes in seasonal sea ice distribution and productivity in the Sea of Okhotsk during the deglaciations. Geochemistry, Geophysics, Geosystems 10 (10), Q10007. https://doi.org/10.1029/2009GC002613.

Seki, O., Harada, N., Sato, M., Kawamura, K., Ijiri, A., Nakatsuka, T., 2012. Assessment for paleoclimatic utility of terrestrial biomarker records in the Okhotsk Sea sediments. Deep Sea Research II 61–64, 85–92. https://doi.org/10.1016/j.dsr2.2011.03.008.

Seki, O., Bendle, J.A., Harada, N., Kobayashi, M., Sawada, K., Moossen, H., Inglis, G.N., Naga, S., Sakamoto, T., 2014a. Assessment and calibration of TEX86 paleothermometry in the Sea of Okhotsk and sub-polar North Pacific region Implications for paleoceanography. Progress in Oceanography 126, 254–266. https://doi.org/10.1016/j.pocean.2014.04.013.

Seki, O., Mikami, Y., Bendle, J.A., Nakatsuka, T., Kim, V.I., Shesterkin, V.P., Makinov, A. N., Fukushima, M., Moossen, H.M., Shouten, S., 2014b. Lignin phenols and BIT index distributions in the Amur River and the Sea of Okhotsk Implications for the source and transport of particulate terrestrial organic matter to the ocean. Progress in Oceanography 126, 146–154. https://doi.org/10.1016/j.pocean.2014.05.003.

Shackleton, N.J., Opdyke, N.D., 1976. Oxygen-isotope and paleomagnetic stratigraphy of Pacific core V28–239: Late Pliocene to latest Pleistocene. Geological Society of America Memoir 145, 449–464. https://doi.org/10.1130/MEM145-p449.

Siddall, M., Bard, E., Rohling, E.J., Hemleben, C., 2006. Sea-level reversal during Termination II. Geology 34, 817. https://doi.org/10.1130/G22705.1.

Sinninghe Damsté, J.S., Rampen, S., Rijpstra, W.I.C., Abbas, B., Muyzer, G., Schouten, S., 2003. A diatomaceous origin for long-chain diols and mid-chain hydroxy methyl alkanoates widely occurring in Quaternary marine sediments: Indicators for high nutrient conditions. Geochimica and Cosmochimica Acta 67, 1339–1348. https://doi.org/10.1016/S0016-7037(02)01225-5.

Smith, M., De Deckker, P., Rogers, J., Brocks, J., Hope, J., Schmidt, S., dos Santos, R.L., Schouten, S., 2013. Comparison of U37K′, TEX86H and LDI temperature proxies for reconstruction of south-east Australian ocean temperatures. Organic geochemistry 64, 94–104. https://doi.org/10.1016/j.orggeochem.2013.08.015.

Sorokin, Y.I., Sorokin, P.Y., 1999. Production in the Sea of Okhotsk? Journal of Plankton Research 21 (2), 201–230.

St. John, K.E., Krissek, L.A., 1999. Regional patterns of Pleistocene ice-rafted debris flux in the North Pacific. Paleoceanography 14 (5), 653–662. https://doi.org/10.1029/1999PA900030.

Sundström, B.G., 1986. The Marine Diatom Genus Rhizosolenia: A New Approach to the Taxonomy. Ph.D. dissertation. Lund University, Lund, Sweden, 117 pp.

Ternois, Y., Kawamura, K., Keigwin, L., Okhouchi, N., Nakatsuka, T., 2001. A biomarker approach for assessing marine and terrigenous inputs to the sediments of Sea of Okhotsk for the last 27,000 years. Geochimica and Cosmochimica Acta 65 (5), 791–802. https://doi.org/10.1016/S0016-7037(00)00598-6.

Thomas, E.K., Clemens, S.C., Sun, Y., Prell, W.L., Huang, Y., Gao, L., Loomis, S., Chen, G., Liu, Z., 2016. Heterodynes dominate precipitation isotopes in the East Asian monsoon region, reflecting interaction of multiple climate factors. Earth and Planetary Science Letters 455, 196–206. https://doi.org/10.1016/j.epsl.2016.09.044.

Thomsen, C., Schulz-Bull, D.E., Petrick, G., Duinker, J.C., 1998. Seasonal variability of the long-chain alkenone flux and the effect on the $U^{k'}_{37}$-index in the Norwegian Sea. Organic Geochemistry 28 (5), 311–323. https://doi.org/10.1016/S0146-6380(98)00003-5.

Tsoy, I.B., Obrezkova, M.S., Artemova, A.V., 2009. Diatoms in surface sediments of the Sea of Okhotsk and the northwest Pacific Ocean. Oceanology 49 (1), 130–139. https://doi.org/10.1134/S0001437009010159.

Tsunogai, S., Ono, T., Watanabe, S., 1992. Increase in total carbonate in the western North Pacific water and a hypothesis on the missing sink of anthropogenic carbon. Journal of Oceanography 49, 305–315. https://doi.org/10.1007/BF02269568.

van der Meer, M.T., Baas, M., Rijpstra, W.I.C., Marino, G., Rohling, E.J., Damsté, J.S.S., Schouten, S., 2007. Hydrogen isotopic compositions of long-chain alkenones record freshwater flooding of the Eastern Mediterranean at the onset of sapropel deposition. Earth and Planetary Science Letters 262 (3–4), 594–600. https://doi.org/10.1016/j.epsl.2007.08.014.

van der Meer, M.T.J., Benthien, A., Bijma, J., Schouten, S., Sinninghe Damsté, J., 2013. Alkenone distribution impacts the hydrogen isotopic composition of the C37:2 and C37:3 alkan-2-ones in Emiliania huxleyi. Geochimica and Cosmochimica Acta 111, 162–166. https://doi.org/10.1016/j.gca.2012.10.041.

Volkman, J.K., Barrett, S.M., Dunstan, G.A., Jeffrey, S.W., 1992. C30–C32 alkyl diols and unsaturated alcohols in microalgae of the class Eustigmatophyceae. Organic Geochemistry 18, 131–138.

Waelbroeck, C., Labeyrie, L., Michel, E., Duplessy, J.C., McManus, J.F., Lambeck, K., Blabon, E., Labracherie, M., 2002. Sea-level and deep water temperature changes derived from benthic foraminifera isotopic records. Quaternary Science Reviews 21 (1–3), 295–305. https://doi.org/10.1016/S0277-3791(01)00101-9.

Wang, P., Tian, J., Cheng, X., Liu, C., Xu, J., 2003. Carbon reservoir changes preceded major ice-sheet expansion at the mid-Brunhes event. Geology 31 (3), 239–242. https://doi.org/10.1130/0091-7613(2003)031<0239:CRCPMI>2.0.CO;2.

Wang, W.-L., Wang, L.-C., 2008. Reconstruction of Oceanographic Changes Based on the Diatom records of the central Okhotsk Sea over the last 50000 years. Terrestrial, Atmospheric & Oceanic Sciences. 19 (4), 403–411. https://doi.org/10.3319/TAO.2008.19.4.403(IMAGES).

Warnock, J.P., Bauersachs, T., Kotthoff, U., Brandt, H.T., Andrén, E., 2017. Holocene environmental history of the Ångermanälven Estuary, northern Baltic Sea. Boreas 47 (2), 593–608. https://doi.org/10.1111/bor.12281.

Weijers, J.W.H., Panoto, E., van Bleijswijk, J., Schouten, S., Rijpstra, W.I.C., Balk, M., Stams, A.J.M., Sinninghe Damsté, J.S., 2009. Constraints on the biological source (s) of the orphan branched tetraether membrane lipids. Geomicrobiology Journal 26, 402–414. https://doi.org/10.1080/01490450902937293.

Weiss, G.M., Pfannerstill, E.Y., Schouten, S., Sinninghe Damsté, J.S., van der Meer, M. T., 2017. Effects of alkalinity and salinity at low and high light intensity on hydrogen isotope fractionation of long-chain alkenones produced by Emiliania huxleyi. Biogeosciences 14 (24), 5693–5704. https://doi.org/10.5194/bg-14-5693-2017.

Willmott, V., Rampen, S., Domack, E., Canals, M., Sinninghe Damsté, J., Schouten, S., 2010. Holocene changes in Proboscia diatom productivity in shelf waters of the north-western Antarctic Peninsula. Antarctic Sciences 22, 3–10. https://doi.org/10.1017/S095410200999037X.

Zell, C., Kim, J.H., Moreira-Turcq, P., Abril, G., Hopmans, E.C., Bonnet, M.P., Lima Sobrinho, R., Sinninghe Damsté, J.S., 2013. Disentangling the origins of branched tetraether lipids and crenarchaeol in the lower Amazon River: implications for GDGT-based proxies. Limnology and Oceanography 58 (1), 343–353. https://doi.org/10.4319/lo.2013.58.1.0343.

Zell, C., Kim, J.H., Dorhout, D., Baas, M., Sinninghe Damsté, J.S., 2015. Sources and distributions of branched tetraether lipids and crenarchaeol along the Portuguese continental margin: implications for the BIT index. Continental Shelf Research 96, 34–44. https://doi.org/10.1016/j.csr.2015.01.006.

Zhu, X., Jia, G., Mao, S., Wen, Y., 2018. Sediment records of long chain alkyl diols in an upwelling area of the coastal northern South China Sea. Organic Geochemistry 121, 1–9. https://doi.org/10.1016/j.orggeochem.2018.03.014.